Impact of Kara Sea landfast ice extent on the stability of the pan-Arctic halocline

Yuqing Liu[1], Martin Losch[2], and Bruno Tremblay[3]

[1]Alfred-Wegener-Institut Helmholtz-Zentrum für Polar- und Meeresforschung
[2]Alfred Wegener Institute for Polar and Marine Research
[3]McGill University

May 25, 2023

Abstract

Landfast ice is immobile sea ice attached to the coastline. Through the position of wintertime offshore polynyas and related brine rejection with new ice formation, the landfast ice cover has an effect on the halocline stability in the Arctic. Landfast ice formation depends in large part on the depth of the ocean floor. Numerical simulations with and without a landfast ice cover in the relatively deeper Kara Sea show that the presence of landfast ice decreases the near-surface salinity not only locally, but the local negative salinity anomaly in the Kara Sea is then advected in the Makarov Basin on timescales of less than ten years. The fresh signal is also affected by river discharge into the Kara Sea. We argue that a proper representation of landfast ice in the Kara is key to a proper simulation of the halocline stability and Atlantification of the Makarov Basin.

Impact of Kara Sea landfast ice extent on the stability of the pan-Arctic halocline

Yuqing Liu[1], Martin Losch[1], Bruno Tremblay[2]

[1]Alfred-Wegener-Institut, Helmholtz-Zentrum für Polar-und Meeresforschung, Bremerhaven, Germany

[2]Department of Atmospheric and Oceanic Sciences, McGill University, Montreal, Quebec, Canada

Key Points:

- The extent of landfast ice in the Kara Sea has a significant impact on the upper ocean salinity.
- This fresh upper ocean signal is advected from the Kara Sea to the central Arctic
- The salt anomaly advection from the ice and upper ocean affects the stability of the halocline of the Makarov Basin.

Corresponding author: Yuqing Liu, `Yuqing.Liu@awi.de`

Abstract

Landfast ice is immobile sea ice attached to the coastline. Through the position of wintertime offshore polynyas and related brine rejection with new ice formation, the landfast ice cover has an effect on the halocline stability in the Arctic. Landfast ice formation depends in large part on the depth of the ocean floor. Numerical simulations with and without a landfast ice cover in the relatively deeper Kara Sea show that the presence of landfast ice decreases the near-surface salinity not only locally, but the local negative salinity anomaly in the Kara Sea is then advected in the Makarov Basin on timescales of less than ten years. The fresh signal is also affected by river discharge into the Kara Sea. We argue that a proper representation of landfast ice in the Kara is key to a proper simulation of the halocline stability and Atlantification of the Makarov Basin.

Plain Language Summary

Landfast ice is sea ice that forms a stable ice cover attached to the coast. In the Arctic, this land extension serves as a platform for hunting, tourism, scientific observation, oil and gas drilling. Landfast ice also influences the distribution of temperature and salinity in the Arctic Ocean because it sets the areas where new ice is formed from seawater. This process leaves more saline and denser surface water behind. Most marginal seas in the Arctic Ocean are very shallow, except for the Kara Sea where the water depth can reach 60 m implying that the effect of landfast ice on the ocean can be different than in the other marginal seas. In a numerical computer model of the Arctic Ocean with sea ice, these effects are explored. With more landfast ice prevents new ice formation and leads to lower salinity, that is, fresher water, locally. Only for the Kara Sea, the fresh signal in the surface ocean is exported to the central Arctic Ocean, where it leads to a more stable stratification. This effect may have implications for the water mass structure in a future Arctic Ocean.

1 Introduction

Landfast ice (also called fast ice) is defined as "sea ice that stays fast along the coast where it is attached to the shore, to an ice wall, to an ice front, over shoals, or between grounded icebergs" (World Meteorological Organization, 1970). Landfast ice can extend a few kilometers (e.g. Beaufort Sea, Western Laptev Sea) to several hundred kilometers into the ocean (e.g. Kara Sea, East Siberian Sea, Eastern Laptev Sea). Landfast ice formation is related to local bathymetry and coastline geometry. It can be grounded on the ocean floor by pressure ridges (Stamukhi) in shallow water and over shoals (Mahoney et al., 2014; Lemieux et al., 2015, 2016), attached to coastlines by frictional effects, or pinned by offshore islands (Divine et al., 2005). Landfast ice plays an important role in polar coastal regions. The stable landfast ice cover decreases the energy, momentum, and heat flux between the atmosphere and the ocean (Johnson et al., 2012; Lemieux et al., 2016). Consequently, ocean mixing underneath a landfast ice cover is reduced. The stable fast ice cover also prevents sea ice compression in convergent motion, thus limiting sea ice thickness (Johnson et al., 2012; Itkin et al., 2015). The northward extent of landfast ice determines the location of flaw lead polynyas (i.e. the openings between the landfast ice and pack ice). The position of these polynyas is important for the large scale Arctic hydrography, because salt rejection during ice formation in these polynyas leads to dense bottom water that flows off the continental shelves, decoupling the warm Atlantic water from the cold surface water with effects on the Arctic halocline stability (Itkin et al., 2015).

The stratification in the Arctic Ocean is mainly determined by salinity instead of temperature (i.e. there is a halocline instead of a thermocline, Timmermans & Marshall, 2020). The salt budget in the Arctic Ocean is a function of lateral processes, such as advection of relatively saline Atlantic water and fresh Pacific water, river runoff, and local (vertical) processes, such as ice melt and formation, evaporation and precipitation (Rudels et al., 1994; Serreze et al., 2006; Morison et al., 2012; Haine et al., 2015; Proshutinsky et al., 2015). Here, we focus on changes in salinity due to changes in landfast ice area and how this affects the halocline stability in the Arctic. We explore the effects of different landfast ice regions on the salinity in the upper ocean and show that this effect can be particularly large for landfast ice in the relatively deep Kara Sea ($\sim$60 m). To this end, we exploit parameterizations that lead to more landfast ice (Lemieux et al., 2015; Liu et al., 2022) as a switch to turn on and off landfast ice in different regions. Different sensitivity experiments and a detailed salt budget analysis shed light on which landfast ice areas cause which of the changes in the large-scale salinity distribution.

The paper is organized as follows: the model configuration is described in Section 2, the model results are presented in Section 3, and the discussion and conclusion are given in Section 4 and Section 5.

2 Model and Experimental set-up

We use a regional Arctic configuration of the Massachusetts Institute of Technology general circulation model (MITgcm, Marshall et al., 1997; MITgcm Group, 2022) with a grid resolution of 36 km. This model resolves ocean and sea ice processes with a finite-volume discretization on an Arakawa C grid. The sea ice component includes a zero-layer thermodynamics (Semtner, 1976) and viscous-plastic dynamics with an elliptical yield curve and a normal flow rule (Hibler, 1979; Zhang & Hibler, 1997). The surface forcing is from global atmospheric reanalysis ERA-Interim data (Dee et al., 2011). The hydrography is initialized with temperature and salinity fields from the Polar Science Center Hydrographic Climatology 3.0 (Steele et al., 2011). Details of the sea ice model can be found in Losch et al. (2010); Ungermann and Losch (2018).

The model is run from 2001 to 2015 with and without fast ice parameterizations. The first five years constitute a spin-up during which the sea ice and surface ocean reaches a stable state for analysis. As in any sea-ice ocean model at this resolution, the landfast ice cover in marginal seas is too small; implementing a basal drag parameterization

(Lemieux et al., 2015) leads to realistic landfast ice areas in shallow marginal seas such as the Beaufort, Laptev and the East Siberian Seas, but not in the Kara Sea. The extent of the fast ice in the Kara Sea can be improved in part by implementing a different parameterization where an explicit lateral drag that depends on the sub-grid-scale coastline length and orientation replaces the no-slip boundary condition of the sea-ice momentum equations (Liu et al., 2022). We label the three configurations as CTRL (without any fast ice parameterization), BD (with basal drag parameterization, i.e. fast ice in shallow regions and no fast ice in the Kara Sea), and LD+BD (with both lateral and basal drag parameterization, i.e. most realistic fast ice distribution both in shallow and deep regions). Switching between the BD and the LD+BD configuration allows us to isolate the effect of the landfast ice in the Kara Sea on the Arctic hydrography.

3 Results

3.1 More landfast ice in the Kara Sea, fresher surface water in the interior Arctic

More landfast ice makes the shelves fresher, but more landfast ice in the Kara Sea also makes the interior Arctic fresher (Figure 1c-d). In the landfast ice regions of the Beaufort, East Siberian, Laptev and Kara Seas, the ice concentration is higher (less open water for sea ice formation) along the coastlines with the landfast ice parameterizations, but lower (more open water for more sea ice formation in flaw polynyas) offshore (Figure 1b, see also Itkin et al., 2015, where this effect is restricted to the first three very shallow seas). Especially in the landfast ice regions of the Laptev and East Siberian Seas, this leads to fresher surface water in the simulations with fast ice parameterization (LD+BD, BD) compared to the CTRL run (Figure 1c-d), because the stable landfast ice cover inhibits new ice formation. As a consequence, less salt is rejected, reducing the salinity of the surface ocean. Northward of the East Siberian Sea landfast ice edge, the upper ocean is more saline in the simulation with basal drag parameterization than in the CTRL sim-

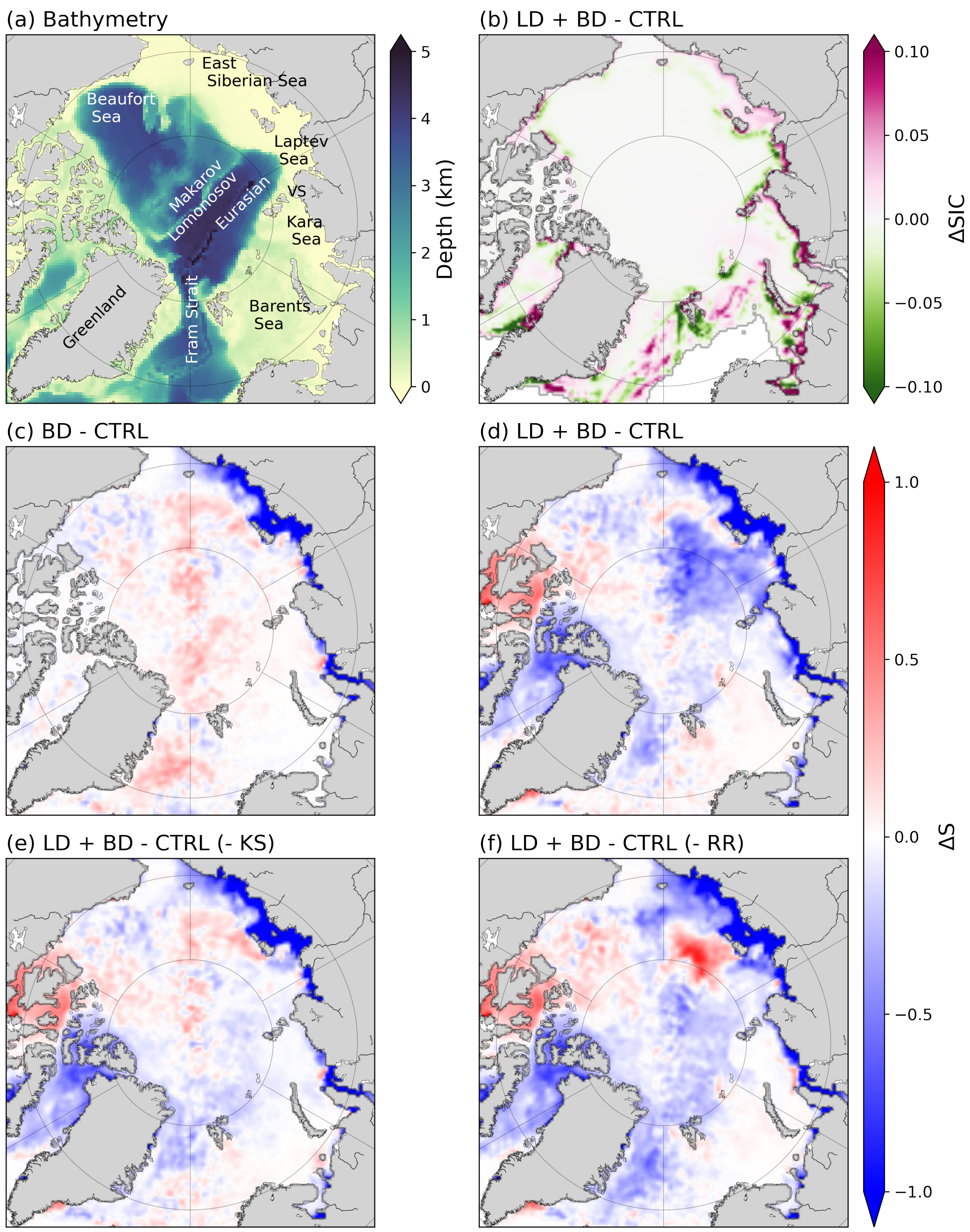

Figure 1. (a) Arctic topography. VS denotes the Vilkitsky Strait. (b) Sea ice concentration difference between LD+BD and CTRL simulations for the mean April of 2006–2015. (c)–(f) Depth averaged (0–40 m) salinity differences for the mean April of 2006–2015 between: (c) the simulation with basal drag parameterization (BD, with landfast ice in the shallow regions) and the CTRL run; (d) the simulation with lateral and basal drag parameterization (LD+BD, with landfast ice in both shallow and deep regions) and the CTRL run; (e) the LD+BD with lateral drag parameterization everywhere except in the Kara Sea and the CTRL run; (f) LD+BD and CTRL simulations as in (d), but without river runoff in the Kara Sea.

ulation (Figure 1c), which is consistent with previous results (Itkin et al., 2015), where the landfast ice parameterization was also depth-dependent and only active in shallow (<30 m) water. During offshore wind events in the East Siberian Sea, new ice formation at the edge of the landfast ice leaves more salt behind and increases the surface ocean salinity in the coastal polynyas. The lateral drag parameterization leads to additional landfast ice in the Kara Sea and around Greenland, where the water is deeper. In contrast to the landfast ice effects in the shallow East Siberian and Laptev Seas, this landfast ice in the deep marginal seas leads to a much fresher upper ocean in the Kara Sea and also Makarov Basin (Figure 1d). We emphasize that the only difference between the BD and LD+BD simulation is the additional landfast ice parameterization in the sea ice component of our model.

Salinity observations in the Arctic are sparse. For example, in the Unified Database for Arctic and Subarctic Hydrography (UDASH, Behrendt et al., 2017; Behrendt et al., 2018), there are only 28 salinity casts in all Aprils of 2006–2015 in the region between the meridians 120°E and 180°E and north of 75°N (approximately the Makarov Basin). Of these 28 casts, only 20 contain data in the upper 40 m. We compare the average over the top 40 m to the corresponding model grid points and find that the root-mean-square difference (RMSD) of salinity between the LD+BD run and the UDASH data (1.06) is smaller than the value between the CTRL run and the UDASH data (1.27). This shows that the extra fast ice in the Kara Sea and the consequential negative salinity anomaly in the Makarov Basin slightly, and maybe fortuitously, reduces a model bias (plots not shown).

In two sensitivity experiments, we turned off the lateral drag parameterization in the LD+BD simulation in the Kara Sea (LD + BD - KS, Figure 1e) and the Greenland Sea and the Canadian Arctic Archipelago separately by setting the coefficient of the lateral drag parameterization to zero in these regions. The fresh upper ocean signal in the Makarov and Eurasian Basins disappears when there is no landfast ice in the Kara Sea

(Figure 1e), whereas the fresh signal in the upper ocean near the Canadian Arctic Archipelago (CAA) and the Greenland Sea disappears when turning off the lateral drag parameterization locally along these coasts (not shown). In a different sensitivity experiment we disabled the river runoff from the Ob and Yenisei Rivers in the Kara Sea aiming to identify the source for the fresher upper ocean signal in the central Arctic (Figure 1f). The amplitude of the negative salinity anomaly in the Kara Sea and the Makarov Basin decreases without river runoff in the Kara Sea and a positive anomaly appears north of the New Siberian Island (Figure 1f). Furthermore, the positive salinity anomaly north of the East Siberian Sea intensifies. We hypothesize that the river runoff contributes to the transport of the low salinity signal in the upper ocean from the Kara Sea to the Makarov Basin (Figure 2).

We trace the river runoff of the Ob and Yenisei Rivers in the Kara Sea with a passive tracer. The passive tracer leaves the Kara Sea through the Vilkitsky Strait (between the Laptev and Kara Seas), then part of the tracer enters the Laptev Sea, and the rest subducts into the Amundsen Basin, passes the Lomonosov Ridge and enters the Makarov Basin. Over the Lomonosov Ridge, Ob/Yenisei water outcrops at the surface and submerges to 50 m in the Makarov Basin (Figure 2). The passive tracer of the Ob and Yenisei water has a similar distribution to the observed Ob/Yenisei water based on chemical tracer-based water mass analyses (Paffrath et al., 2021). The tracer pattern is very similar to the pattern of the low salinity signal in the upper ocean implying a transport path from the Kara Sea to the Makarov Basin.

3.2 Propagation of the low salinity signal

A Hovmöller diagram of the depth-averaged (0–40 m) salinity and salinity difference between different experiments along the transect in Figure 2a illustrates the transport of the low salinity signal from the Kara Sea to the Chuckchi Sea (Figure 3). The positive salinity difference between the BD and CTRL simulations in the Makarov Basin (approximately 1900 km away from the Kara Sea) develops locally very soon after 2001

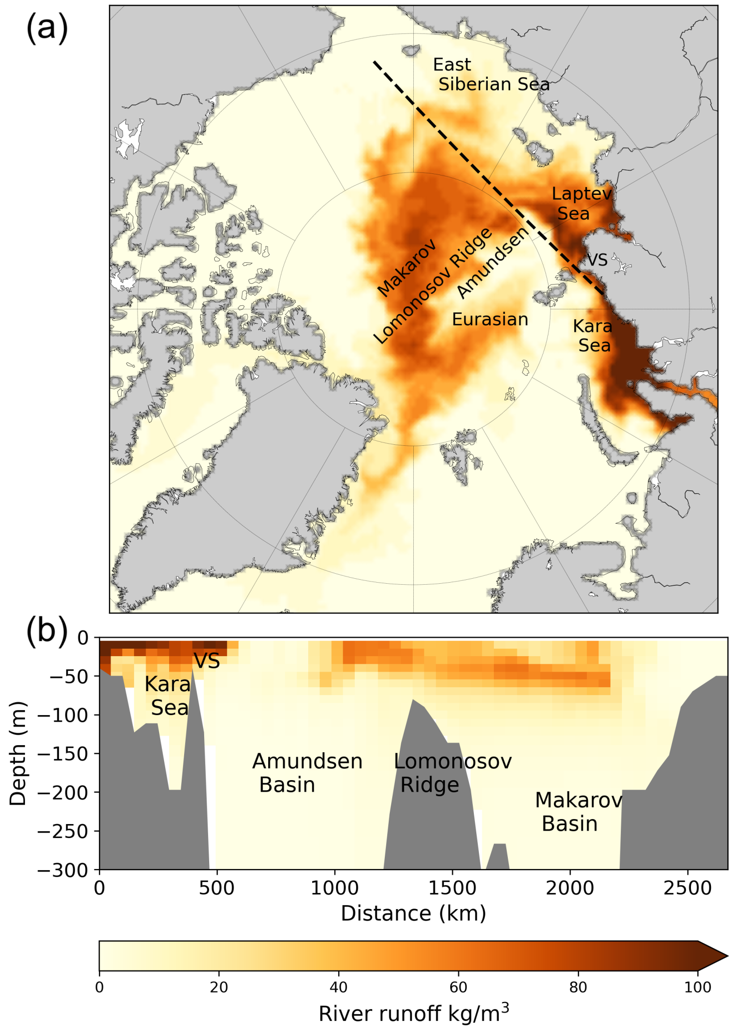

Figure 2. (a) Depth averaged (0–40 m) passive tracer of the river runoff from the Kara Sea in April 2015. (b) Vertical distribution of the passive tracer along the section in panel (a) starting from the Kara Sea to the Chukchi Sea.

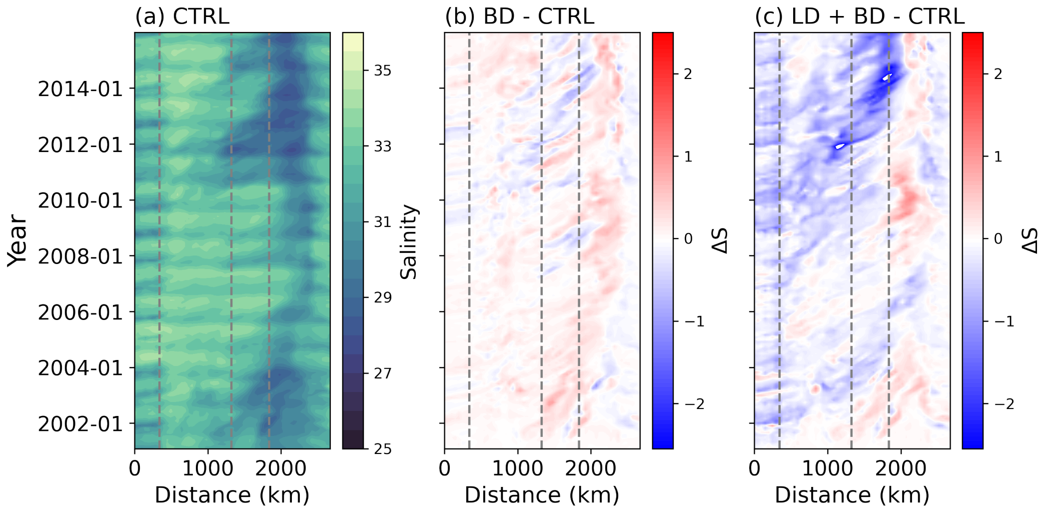

Figure 3. Hovmöller diagram for years 2001 to 2015 of depth-averaged (0–40m) (a) salinity in the CTRL simulation; (b) salinity difference between the BD and CTRL simulations; (c) salinity difference between the LD+BD and CTRL simulations. The abscissa is the distance in km along the transect in Figure 2a. The dashed lines parallel to the ordinate indicate the locations of the Vilkitsky Strait, the Eurasian and the Makarov Basins.

(Figure 3b), when the new ice formation releases salt in the upper ocean in the polynyas north of the East Siberian Sea landfast ice edge. The same positive salinity anomaly also appears in the LD+BD simulation in the Makarov Basin (Figure 3c). In contrast to the locally generated signal, the low salinity signal in the LD+BD simulation in the Makarov and Eurasian Basins is advected from the Kara Sea, apparently starting in 2008, with a negative salinity anomaly peak in 2012. Note the pulses of negative salinity anomaly in the upper ocean moving from the Kara Sea to the Makarov Basin throughout the years 2001-2007. The explanation for the events is elaborated in Section 4.

3.3 Salt budget analysis

Integrating the salt conservation equation leads to a salt budget equation. The change in salt content over time (G^S_{tot}) is equal to the convergence of the advective (G^S_{adv}) and diffusive fluxes (G^S_{diff}), and a forcing term associated with surface salt exchanges (G^S_{forc}):

$$\underbrace{\frac{\partial s}{\partial t}}_{G^S_{\text{tot}}} = \underbrace{-\rho \oint_A uS\,da}_{G^S_{\text{adv}}} + \underbrace{\rho \iiint F_{\text{diff}}\,dx\,dy\,dz}_{G^S_{\text{diff}}} + \underbrace{\rho \iint F_{\text{forc}}\,dx\,dy}_{G^S_{\text{forc}}}, \quad (1)$$

where $\mathbf{u}$ is the ocean velocity normal to the area, S is the salinity, $s = \rho \iiint S\,dx\,dy\,dz$ is the salt content (in grams), da is the area element, A is the surface area of the volume integral. The differences between the simulation with landfast ice and the CTRL run in the advection and salinity tendency in the Arctic Ocean are small for the first five years until the end of 2005 (Figure 4). The trend of the influence of landfast ice in the deep region gradually intensifies after 2006, and the trend stabilizes after the year 2014. The salt content difference in the Arctic Ocean with landfast ice parameterization is determined by surface forcing, advection, and diffusion. The decrease in salt content in the Arctic Ocean in the simulation with fast ice in shallow and deep regions is to 90% caused by changes in advective salt flux through the open boundaries (Figure 4). Furthermore, the remaining 10% of reduced salinity is mainly caused by the surface forcing. The surface forcing flux difference between the LD+BD and CTRL simulation in the Arctic Ocean has a strong seasonal signal governed by the sea ice formation and melt. For perspective, the total salt loss in the Makarov Basin in the upper 40 m is approximately 1.94 Gt per year.

4 Discussion

The presence of landfast ice in sea ice-ocean models changes the position of offshore polynyas and hence the location where sea ice is formed over open water. The modified freshwater flux changes the salinity forcing which in turn leads to changes in the halocline stability in the Arctic (Itkin et al., 2015). This result was obtained with a numerical model that did not have any landfast ice in the Kara Sea. We used a lateral drag parameterization designed to make the Kara Sea landfast ice cover more realistic (Liu et al., 2022) as a switch. When switched on, there is more landfast ice in the Kara Sea, but the landfast ice cover in other fast ice regions does not change very much (Liu et al.,

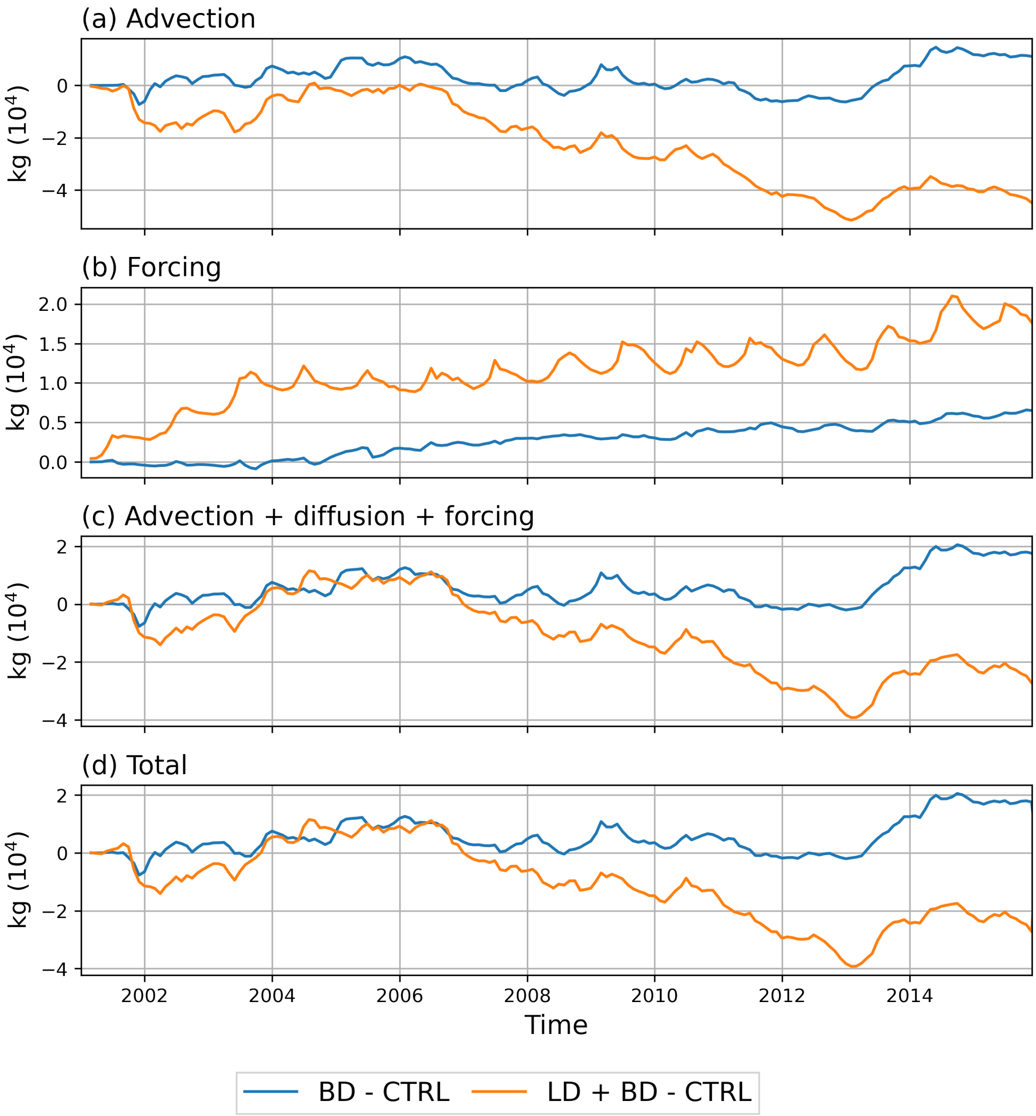

Figure 4. Time series of accumulated salt budget differences ($\int_0^t G(t')\,dt'$, see Eq. 1) in the Arctic Ocean in 2001-2015. The blue line is the difference between BD and CTRL simulation (effects from landfast ice in the shallow region), and the orange line is the difference between LD+BD and CTRL simulation (effects of fast ice in both shallow and deep regions). (a) Advection. (b) Surface forcing (evaporation-precipitation-runoff). (c) The sum of surface forcing, advection and diffusion. (d) Total salt content tendency in the Arctic Ocean. Positive means increasing salinity in the ocean. The (vertical) diffusion term is very small, thus not shown in the plot.

2022). This makes it possible to isolate the effects of the Kara Sea landfast ice. The effect on the near-surface salinity is much larger than including landfast ice in the other marginals seas (Laptev, East Siberian, Beaufort Sea), even though the Kara Sea area is small compared to the other marginal seas. For the halocline, the large decrease of salinity in the top 40 m of the water column means increased stability (and it corrects a saline model bias). Likewise, less landfast ice in the Kara Sea (e.g., in response to climate change), may lead to reduced stability in the central Arctic Ocean and hence an accelerated "Atlantification" as it may become easier for warm Atlantic water to reach the surface (Asbjørnsen et al., 2020; Ingvaldsen et al., 2021), with significant consequences for the sea ice cover extent and seasonality.

Although the negative salinity anomaly in the upper ocean in the simulation with fast ice in the Kara Sea travels from the Kara Sea to the Makarov Basin soon after the start of the model run, there are two main transport episodes (2002–2006 and 2008–2015). These may be driven by the wind forcing in the Arctic (Duan et al., 2019; Zatsepin et al., 2017). The negative salinity difference in the upper ocean is largest after the end of summer in 2012 (Figure 3c), presumably because of the large sea ice retreat in 2012. In August 2012, an intense storm increased mixing in the ocean boundary layer, increased upward ocean heat transport, causing bottom melt, and reduced the sea ice volume about twice as fast as in other years (Zhang et al., 2013). Eventually, the sea ice extent at the end of the summer in 2012 was smaller than it had been in the previous 33 years (Parkinson & Comiso, 2013). The processes are also at play in our simulation and the mean simulated sea ice extent reaches its lowest value of the simulation in 2012 (not shown). More landfast ice melting in the LD+BD simulation reduces the salinity in the upper ocean compared to the CTRL simulation. The increased mixing and melting increase the negative salinity difference. The particularly fresh upper ocean in 2012 may also be related to position of the Beaufort Gyre. As a major freshwater reservoir for the Arctic Ocean, the gyre extended northward after 2012, thus increasing the freshwater content in the Makarov Basin, and making the central Arctic Ocean fresher (Bertosio et al., 2022).

The Kara Sea receives freshwater discharge from the Ob and Yenisei Rivers, which carry over one-third of the total freshwater discharge in the Arctic (Janout et al., 2015). The geostrophic surface currents determine the circulation pathways of river runoff, and of surface water originally from the Pacific and the Atlantic Oceans (Wang et al., 2021). The simulated passive tracer for Ob/Yenisei water agrees with the observed Ob/Yenisei water distribution (Laukert et al., 2017; Paffrath et al., 2021). The tracer experiment demonstrates that the river runoff and the negative salinity anomaly in the upper ocean induced by the fast ice in the Kara Sea travel from the Kara Sea to the Makarov Basin via the Vilkitsky Strait. The exact mechanism by which the river runoff in the Kara Sea modifies the influence the landfast ice has on the hydrography cannot be extracted from the numerical model because the Ob/Yenisei water is stored in landfast ice during sea ice formation and the riverine heat, which is not taken into account in our model, is assumed to be important to explain the phenomena (Janout et al., 2020).

The Arctic mixed layer is important to physical, chemical, and biological processes. Mixed layer properties also influence ocean stratification, sea ice distribution, and heat transfer between ocean, sea ice, and atmosphere. Peralta-Ferriz and Woodgate (2015) suggested two drivers for seasonal mixed layer depth change: sea ice thermodynamics (i.e., salt rejection during ice formation, freshwater input during the ice melt) and wind-driven mixing. During ice-free phases, wind-driven mixing deepens the mixed layer, while thermodynamic processes dominate the stratification and control mixed layer depth variability in winter. With more fast ice less salt is released into the ocean which may modify the mixed layer depth. Our model configuration has 50 vertical layers with a minimum thickness of 10 m in the upper ocean, which is insufficient to explore the details of the influence of landfast ice parameterization on the mixed layer depth. Vertical grid refinement in the upper ocean would allow studying the mixed layer variability difference with and without the landfast ice parameterization.

A proper representation of the landfast ice distribution, as suggested here, may be even more important in the Southern Ocean than in the Arctic Ocean. Along the deep Southern Ocean shelf around Antarctica, landfast ice is mainly attached to grounded icebergs or other coastal features (e.g. the shoreline, glacier tongues, and ice shelves, Fraser et al., 2012, 2020). Salt rejection during continuous sea-ice formation (in polynyas) on the shelves produces the densest waters observed in the world ocean, which eventually are a source of Antarctic Bottom water (Williams et al., 2010; Ohshima et al., 2013, 2016). The dense bottom water is an important part of the global circulation (Killworth, 1983; Nihashi & Ohshima, 2015; Ohshima et al., 2016). In this sense, the impact of realistically simulated landfast ice around Antarctica may even be larger than in the Arctic Ocean where the hydrographic processes appear to be restricted mainly to surface waters.

5 Conclusion

More landfast ice in the Arctic Ocean decreases the upper ocean salinity locally on the shelves in the Kara, Laptev and East Siberian Seas. The largest effect, however, is found for the Kara Sea, where the large fresh upper ocean signal induced by the landfast ice is transported to the central Arctic Ocean and leads to surprisingly large salinity anomaly which increases the halocline stability. River runoff in the Kara Sea contributes to transporting the signal from the Kara Sea to the Makarov Basin. The negative salinity tendency with the landfast ice in both shallow and deep shelves can be attributed mainly (90%) to advective fluxes out of the Arctic Ocean and to surface forcing (10%).

A sea ice model with a proper representation of landfast ice will improve our understanding of its influence on the hydrography in the Arctic. The landfast ice occurrence modifies sea ice thermodynamics and thus may reshape the mixed layer depth. A finner vertical resolution model is suggested to investigate further the impact of landfast ice presentation on the mixed layer depth. Implementing landfast ice parameterizations in sea ice model of the Antarctic will allow to explore the effects of landfast ice on the Antarctic Bottom Water formation.

Open Research

The model data in this manuscript is based on the Massachusetts Institute of Technology general circulation model (MITgcm, MITgcm Group, 2022), the version with lateral drag parameterization is available at `https://doi.org/10.5281/zenodo.7954400` and the model configurations at `https://doi.org/10.5281/zenodo.7919422`. The salinity in the Unified Database for Arctic and Subarctic Hydrography (UDASH) is available from the PANGAEA data archive (Behrendt et al., 2017). Figures are made with Matplotlib version 3.1.3 (Hunter, 2007), available under the Matplotlib license at `https://matplotlib.org/`.

Acknowledgments

The authors thank Markus Janout, Thomas Jung, and Lars Kaleschke for constructive discussions. This work is supported by the DFG-funded International Research Training Group ArcTrain (IRTG 1904 ArcTrain).

References

Asbjørnsen, H., Årthun, M., Skagseth, Ø., & Eldevik, T. (2020). Mechanisms underlying recent Arctic Atlantification. *Geophysical research letters*, *47*(15), e2020GL088036. doi: 10.1029/2020GL088036

Behrendt, A., Sumata, H., Rabe, B., & Schauer, U. (2017). *A comprehensive, quality-controlled and up-to-date data set of temperature and salinity data for the Arctic Mediterranean Sea (Version 1.0)* [data set]. PANGAEA. doi: 10.1594/PANGAEA.872931

Behrendt, A., Sumata, H., Rabe, B., & Schauer, U. (2018). UDASH–Unified Database for Arctic and Subarctic Hydrography. *Earth System Science Data*, *10*(2), 1119–1138. doi: 10.5194/essd-10-1119-2018

Bertosio, C., Provost, C., Athanase, M., Sennéchael, N., Garric, G., Lellouche, J.-m., … Park, T. (2022). Changes in freshwater distribution and pathways in the Arctic Ocean since 2007 in the Mercator Ocean global operational system. *Journal of Geophysical Research: Oceans*, *127*(6), e2021JC017701. doi: 10.1029/2021JC017701

Dee, D. P., Uppala, S. M., Simmons, A. J., Berrisford, P., Poli, P., Kobayashi, S., … Vitart, F. (2011). The ERA-Interim reanalysis: Configuration and performance of the data assimilation system. *Quarterly Journal of the Royal Meteorological Society*, *137*(656), 553–597. doi: 10.1002/qj.828

Divine, D. V., Korsnes, R., Makshtas, A. P., Godtliebsen, F., & Svendsen, H. (2005). Atmospheric-driven state transfer of shore-fast ice in the northeastern Kara Sea. *Journal of Geophysical Research C: Oceans*, *110*(9), 1–13. doi: 10.1029/2004JC002706

Duan, C., Dong, S., Xie, Z., & Wang, Z. (2019). Temporal variability and trends of sea ice in the Kara Sea and their relationship with atmospheric factors. *Polar Science*, *20*, 136–147. doi: 10.1016/j.polar.2019.03.002

Fraser, A. D., Massom, R. A., Michael, K. J., Galton-Fenzi, B. K., & Lieser, J. L. (2012). East Antarctic landfast sea ice distribution and variability, 2000–08. *Journal of Climate*, *25*(4), 1137–1156. doi: 10.1175/JCLI-D-10-05032.1

Fraser, A. D., Massom, R. A., Ohshima, K. I., Willmes, S., Kappes, P. J., Cartwright, J., & Porter-Smith, R. (2020). High-resolution mapping of circum-Antarctic landfast sea ice distribution, 2000-2018. *Earth System Science Data*, *12*(4), 2987–2999. doi: 10.5194/essd-12-2987-2020

Haine, T. W., Curry, B., Gerdes, R., Hansen, E., Karcher, M., Lee, C., … Woodgate, R. (2015). Arctic freshwater export: Status, mechanisms, and prospects. *Global and Planetary Change*, *125*, 13–35. doi: 10.1016/j.gloplacha.2014.11.013

Hibler, W. D. (1979). A dynamic thermodynamic sea ice model. *Journal of Physical Oceanography*, *9*(4), 815–846. doi: 10.1175/1520-0485(1979)009⟨0815:ADTSIM⟩2.0.CO;2

Hunter, J. D. (2007). Matplotlib: A 2d graphics environment. *Computing in Science & Engineering*, *9*(3), 90–95. doi: 10.5281/zenodo.3633844

Ingvaldsen, R. B., Assmann, K. M., Primicerio, R., Fossheim, M., Polyakov, I. V., & Dolgov, A. V. (2021). Physical manifestations and ecological implications of Arctic Atlantification. *Nature Reviews Earth & Environment*, *2*(12), 874–889. doi: 10.1038/s43017-021-00228-x

Itkin, P., Losch, M., & Gerdes, R. (2015). Landfast ice affects the stability of the Arctic halocline: Evidence from a numerical model. *Journal of Geophysical Research: Oceans*, *120*(4), 2622–2635. doi: 10.1002/2014JC010353

Janout, M. A., Aksenov, Y., Hölemann, J. A., Rabe, B., Schauer, U., Polyakov, I. V., … Timokhov, L. (2015). Kara Sea freshwater transport through Vilkitsky Strait: Variability, forcing, and further pathways toward the western Arctic Ocean from a model and observations. *Journal of Geophysical Research: Oceans*, *120*(7), 4925–4944. doi: 10.1002/2014JC010635

Janout, M. A., Hölemann, J., Laukert, G., Smirnov, A., Krumpen, T., Bauch, D., & Timokhov, L. (2020). On the variability of stratification in the freshwater-influenced Laptev Sea region. *Frontiers in Marine Science*, *7*, 543489. doi: 10.3389/fmars.2020.543489

Johnson, M., Proshutinsky, A., Aksenov, Y., Nguyen, A. T., Lindsay, R., Haas, C., … De Cuevas, B. (2012). Evaluation of Arctic sea ice thickness simulated by Arctic Ocean model intercomparison project models. *Journal of Geophysical Research: Oceans*, *117*(3). doi: 10.1029/2011JC007257

Killworth, P. D. (1983). Deep convection in the World Ocean. *Reviews of Geophysics*, *21*(1), 1–26. doi: 10.1029/RG021i001p00001

Laukert, G., Frank, M., Bauch, D., Hathorne, E. C., Rabe, B., von Appen, W.-J., …

Kassens, H. (2017). Ocean circulation and freshwater pathways in the Arctic Mediterranean based on a combined Nd isotope, REE and oxygen isotope section across Fram Strait. *Geochimica et Cosmochimica Acta*, *202*, 285–309. doi: 10.1016/j.gca.2016.12.028

Lemieux, J. F., Dupont, F., Blain, P., Roy, F., Smith, G. C., & Flato, G. M. (2016). Improving the simulation of landfast ice by combining tensile strength and a parameterization for grounded ridges. *Journal of Geophysical Research: Oceans*, *121*(10), 7354–7368. doi: 10.1002/2016JC012006

Lemieux, J. F., Tremblay, L. B., Dupont, F., Plante, M., Smith, G. C., & Dumont, D. (2015). A basal stress parameterization for modeling landfast ice. *Journal of Geophysical Research: Oceans*, *120*(4), 3157–3173. doi: 10.1002/2014JC010678

Liu, Y., Losch, M., Hutter, N., & Mu, L. (2022). A new parameterization of coastal drag to simulate landfast ice in deep marginal seas in the Arctic. *Journal of Geophysical Research: Oceans*, *127*(6), e2022JC018413. doi: 10.1029/2022JC018413

Losch, M., Menemenlis, D., Campin, J. M., Heimbach, P., & Hill, C. (2010). On the formulation of sea-ice models. Part 1: Effects of different solver implementations and parameterizations. *Ocean Modelling*, *33*(1-2), 129–144. doi: 10.1016/j.ocemod.2009.12.008

Mahoney, A. R., Eicken, H., Gaylord, A. G., & Gens, R. (2014). Landfast sea ice extent in the Chukchi and Beaufort Seas: The annual cycle and decadal variability. *Cold Regions Science and Technology*, *103*, 41–56. doi: 10.1016/j.coldregions.2014.03.003

Marshall, J., Adcroft, A., Hill, C., Perelman, L., & Heisey, C. (1997). A finite-volume, incompressible navier stokes model for, studies of the ocean on parallel computers. *Journal of Geophysical Research C: Oceans*, *102*(C3), 5753–5766. doi: 10.1029/96JC02775

MITgcm Group. (2022). *MITgcm User Manual.* `https://mitgcm.readthedocs.io/`. Cambridge, MA 02139, USA.

Morison, J., Kwok, R., Peralta-Ferriz, C., Alkire, M., Rigor, I., Andersen, R., & Steele, M. (2012). Changing Arctic Ocean freshwater pathways. *Nature*, *481*(7379), 66–70. doi: 10.1038/NATURE10705

Nihashi, S., & Ohshima, K. I. (2015). Circumpolar mapping of Antarctic coastal polynyas and landfast sea ice: Relationship and variability. *Journal of Climate*, *28*(9), 3650–3670. doi: 10.1175/JCLI-D-14-00369.1

Ohshima, K. I., Fukamachi, Y., Williams, G. D., Nihashi, S., Roquet, F., Kitade, Y., ... Wakatsuchi, M. (2013). Antarctic Bottom Water production by intense sea-ice formation in the Cape Darnley polynya. *Nature Geoscience*, *6*(3), 235–240. doi: 10.1038/ngeo1738

Ohshima, K. I., Nihashi, S., & Iwamoto, K. (2016). Global view of sea-ice production in polynyas and its linkage to dense/bottom water formation. *Geoscience Letters*, *3*(1). doi: 10.1186/s40562-016-0045-4

Paffrath, R., Laukert, G., Bauch, D., Rutgers van der Loeff, M., & Pahnke, K. (2021). Separating individual contributions of major Siberian rivers in the Transpolar Drift of the Arctic Ocean. *Scientific Reports*, *11*(1), 1–11. doi: 10.1038/s41598-021-86948-y

Parkinson, C. L., & Comiso, J. C. (2013). On the 2012 record low Arctic sea ice cover: Combined impact of preconditioning and an August storm. *Geophysical Research Letters*, *40*(7), 1356–1361. doi: 10.1002/grl.50349

Peralta-Ferriz, C., & Woodgate, R. A. (2015). Seasonal and interannual variability of pan-Arctic surface mixed layer properties from 1979 to 2012 from hydrographic data, and the dominance of stratification for multiyear mixed layer depth shoaling. *Progress in Oceanography*, *134*, 19–53. doi: 10.1016/j.pocean.2014.12.005

Proshutinsky, A., Dukhovskoy, D., Timmermans, M.-L., Krishfield, R., & Bamber,

J. L. (2015). Arctic circulation regimes. *Philosophical Transactions of the Royal Society A: Mathematical, Physical and Engineering Sciences*, *373*(2052), 20140160. doi: 10.1098/rsta.2014.0160

Rudels, B., Jones, E., Anderson, L., & Kattner, G. (1994). On the intermediate depth waters of the Arctic Ocean. *Washington DC American Geophysical Union Geophysical Monograph Series*, *85*, 33–46.

Semtner, A. J. (1976). A model for the thermodynamic growth of sea ice in numerical investigations of climate. *Journal of Physical Oceanography*, *6*(3), 379–389. doi: 10.1175/1520-0485(1976)006⟨0379:amfttg⟩2.0.co;2

Serreze, M. C., Barrett, A. P., Slater, A. G., Woodgate, R. A., Aagaard, K., Lammers, R. B., … Lee, C. M. (2006). The large-scale freshwater cycle of the Arctic. *Journal of Geophysical Research: Oceans*, *111*(11). doi: 10.1029/2005JC003424

Steele, M., Ermold, W., & Zhang, J. (2011). Modeling the formation and fate of the near-surface temperature maximum in the Canadian Basin of the Arctic Ocean. *Journal of Geophysical Research: Oceans*, *116*(11), 1–13. doi: 10.1029/2010JC006803

Timmermans, M. L., & Marshall, J. (2020). Understanding Arctic Ocean circulation: A review of ocean dynamics in a changing climate. *Journal of Geophysical Research: Oceans*, *125*(4). doi: 10.1029/2018JC014378

Ungermann, M., & Losch, M. (2018). An observationally based evaluation of subgrid scale ice thickness distributions simulated in a large-scale sea ice-ocean model of the Arctic Ocean. *Journal of Geophysical Research: Oceans*, *123*(11), 8052–8067. doi: 10.1029/2018JC014022

Wang, Q., Danilov, S., Sidorenko, D., & Wang, X. (2021). Circulation pathways and exports of Arctic river runoff influenced by atmospheric circulation regimes. *Frontiers in Marine Science*, *8*, 707593. doi: 10.3389/fmars.2021.707593

Williams, G. D., Aoki, S., Jacobs, S. S., Rintoul, S. R., Tamura, T., & Bindoff,

N. L. (2010). Antarctic bottom water from the Adélie and George V Land coast, East Antarctica (140-149°E). *Journal of Geophysical Research: Oceans*, *115*(4), 1–29. doi: 10.1029/2009JC005812

World Meteorological Organization. (1970). *WMO sea-ice nomenclature. Terminology, codes and illustrated glossary* (Tech. Rep.). Geneva: Secretariat of the World Meteorological Organization.

Zatsepin, A., Zavialov, P., Baranov, V., Kremenetskiy, V., Nedospasov, A., Poyarkov, S., & Ocherednik, V. (2017). On the mechanism of wind-induced transformation of a river runoff water lens in the Kara Sea. *Oceanology*, *57*(1), 1–7. doi: 10.1134/S0001437017010222

Zhang, J., & Hibler, W. D. (1997). On an efficient numerical method for modeling sea ice dynamics. *Journal of Geophysical Research: Oceans*, *102*(C4), 8691–8702. doi: 10.1029/96JC03744

Zhang, J., Lindsay, R., Schweiger, A., & Steele, M. (2013). The impact of an intense summer cyclone on 2012 Arctic sea ice retreat. *Geophysical Research Letters*, *40*(4), 720–726. doi: 10.1002/grl.50190

Impact of Kara Sea landfast ice extent on the stability of the pan-Arctic halocline

Yuqing Liu[1], Martin Losch[1], Bruno Tremblay[2]

[1]Alfred-Wegener-Institut, Helmholtz-Zentrum für Polar-und Meeresforschung, Bremerhaven, Germany
[2]Department of Atmospheric and Oceanic Sciences, McGill University, Montreal, Quebec, Canada

Key Points:

- The extent of landfast ice in the Kara Sea has a significant impact on the upper ocean salinity.
- This fresh upper ocean signal is advected from the Kara Sea to the central Arctic
- The salt anomaly advection from the ice and upper ocean affects the stability of the halocline of the Makarov Basin.

Corresponding author: Yuqing Liu, Yuqing.Liu@awi.de

Abstract

Landfast ice is immobile sea ice attached to the coastline. Through the position of wintertime offshore polynyas and related brine rejection with new ice formation, the landfast ice cover has an effect on the halocline stability in the Arctic. Landfast ice formation depends in large part on the depth of the ocean floor. Numerical simulations with and without a landfast ice cover in the relatively deeper Kara Sea show that the presence of landfast ice decreases the near-surface salinity not only locally, but the local negative salinity anomaly in the Kara Sea is then advected in the Makarov Basin on timescales of less than ten years. The fresh signal is also affected by river discharge into the Kara Sea. We argue that a proper representation of landfast ice in the Kara is key to a proper simulation of the halocline stability and Atlantification of the Makarov Basin.

Plain Language Summary

Landfast ice is sea ice that forms a stable ice cover attached to the coast. In the Arctic, this land extension serves as a platform for hunting, tourism, scientific observation, oil and gas drilling. Landfast ice also influences the distribution of temperature and salinity in the Arctic Ocean because it sets the areas where new ice is formed from seawater. This process leaves more saline and denser surface water behind. Most marginal seas in the Arctic Ocean are very shallow, except for the Kara Sea where the water depth can reach 60 m implying that the effect of landfast ice on the ocean can be different than in the other marginal seas. In a numerical computer model of the Arctic Ocean with sea ice, these effects are explored. With more landfast ice prevents new ice formation and leads to lower salinity, that is, fresher water, locally. Only for the Kara Sea, the fresh signal in the surface ocean is exported to the central Arctic Ocean, where it leads to a more stable stratification. This effect may have implications for the water mass structure in a future Arctic Ocean.

1 Introduction

Landfast ice (also called fast ice) is defined as "sea ice that stays fast along the coast where it is attached to the shore, to an ice wall, to an ice front, over shoals, or between grounded icebergs" (World Meteorological Organization, 1970). Landfast ice can extend a few kilometers (e.g. Beaufort Sea, Western Laptev Sea) to several hundred kilometers into the ocean (e.g. Kara Sea, East Siberian Sea, Eastern Laptev Sea). Landfast ice formation is related to local bathymetry and coastline geometry. It can be grounded on the ocean floor by pressure ridges (Stamukhi) in shallow water and over shoals (Mahoney et al., 2014; Lemieux et al., 2015, 2016), attached to coastlines by frictional effects, or pinned by offshore islands (Divine et al., 2005). Landfast ice plays an important role in polar coastal regions. The stable landfast ice cover decreases the energy, momentum, and heat flux between the atmosphere and the ocean (Johnson et al., 2012; Lemieux et al., 2016). Consequently, ocean mixing underneath a landfast ice cover is reduced. The stable fast ice cover also prevents sea ice compression in convergent motion, thus limiting sea ice thickness (Johnson et al., 2012; Itkin et al., 2015). The northward extent of landfast ice determines the location of flaw lead polynyas (i.e. the openings between the landfast ice and pack ice). The position of these polynyas is important for the large scale Arctic hydrography, because salt rejection during ice formation in these polynyas leads to dense bottom water that flows off the continental shelves, decoupling the warm Atlantic water from the cold surface water with effects on the Arctic halocline stability (Itkin et al., 2015).

The stratification in the Arctic Ocean is mainly determined by salinity instead of temperature (i.e. there is a halocline instead of a thermocline, Timmermans & Marshall, 2020). The salt budget in the Arctic Ocean is a function of lateral processes, such as advection of relatively saline Atlantic water and fresh Pacific water, river runoff, and local (vertical) processes, such as ice melt and formation, evaporation and precipitation (Rudels et al., 1994; Serreze et al., 2006; Morison et al., 2012; Haine et al., 2015; Proshutinsky et al., 2015). Here, we focus on changes in salinity due to changes in landfast ice area and how this affects the halocline stability in the Arctic. We explore the effects of different landfast ice regions on the salinity in the upper ocean and show that this effect can be particularly large for landfast ice in the relatively deep Kara Sea ($\sim 60\,\mathrm{m}$). To this end, we exploit parameterizations that lead to more landfast ice (Lemieux et al., 2015; Liu et al., 2022) as a switch to turn on and off landfast ice in different regions. Different sensitivity experiments and a detailed salt budget analysis shed light on which landfast ice areas cause which of the changes in the large-scale salinity distribution.

The paper is organized as follows: the model configuration is described in Section 2, the model results are presented in Section 3, and the discussion and conclusion are given in Section 4 and Section 5.

2 Model and Experimental set-up

We use a regional Arctic configuration of the Massachusetts Institute of Technology general circulation model (MITgcm, Marshall et al., 1997; MITgcm Group, 2022) with a grid resolution of 36 km. This model resolves ocean and sea ice processes with a finite-volume discretization on an Arakawa C grid. The sea ice component includes a zero-layer thermodynamics (Semtner, 1976) and viscous-plastic dynamics with an elliptical yield curve and a normal flow rule (Hibler, 1979; Zhang & Hibler, 1997). The surface forcing is from global atmospheric reanalysis ERA-Interim data (Dee et al., 2011). The hydrography is initialized with temperature and salinity fields from the Polar Science Center Hydrographic Climatology 3.0 (Steele et al., 2011). Details of the sea ice model can be found in Losch et al. (2010); Ungermann and Losch (2018).

The model is run from 2001 to 2015 with and without fast ice parameterizations. The first five years constitute a spin-up during which the sea ice and surface ocean reaches a stable state for analysis. As in any sea-ice ocean model at this resolution, the landfast ice cover in marginal seas is too small; implementing a basal drag parameterization

(Lemieux et al., 2015) leads to realistic landfast ice areas in shallow marginal seas such as the Beaufort, Laptev and the East Siberian Seas, but not in the Kara Sea. The extent of the fast ice in the Kara Sea can be improved in part by implementing a different parameterization where an explicit lateral drag that depends on the sub-grid-scale coastline length and orientation replaces the no-slip boundary condition of the sea-ice momentum equations (Liu et al., 2022). We label the three configurations as CTRL (without any fast ice parameterization), BD (with basal drag parameterization, i.e. fast ice in shallow regions and no fast ice in the Kara Sea), and LD+BD (with both lateral and basal drag parameterization, i.e. most realistic fast ice distribution both in shallow and deep regions). Switching between the BD and the LD+BD configuration allows us to isolate the effect of the landfast ice in the Kara Sea on the Arctic hydrography.

3 Results

3.1 More landfast ice in the Kara Sea, fresher surface water in the interior Arctic

More landfast ice makes the shelves fresher, but more landfast ice in the Kara Sea also makes the interior Arctic fresher (Figure 1c-d). In the landfast ice regions of the Beaufort, East Siberian, Laptev and Kara Seas, the ice concentration is higher (less open water for sea ice formation) along the coastlines with the landfast ice parameterizations, but lower (more open water for more sea ice formation in flaw polynyas) offshore (Figure 1b, see also Itkin et al., 2015, where this effect is restricted to the first three very shallow seas). Especially in the landfast ice regions of the Laptev and East Siberian Seas, this leads to fresher surface water in the simulations with fast ice parameterization (LD+BD, BD) compared to the CTRL run (Figure 1c-d), because the stable landfast ice cover inhibits new ice formation. As a consequence, less salt is rejected, reducing the salinity of the surface ocean. Northward of the East Siberian Sea landfast ice edge, the upper ocean is more saline in the simulation with basal drag parameterization than in the CTRL sim-

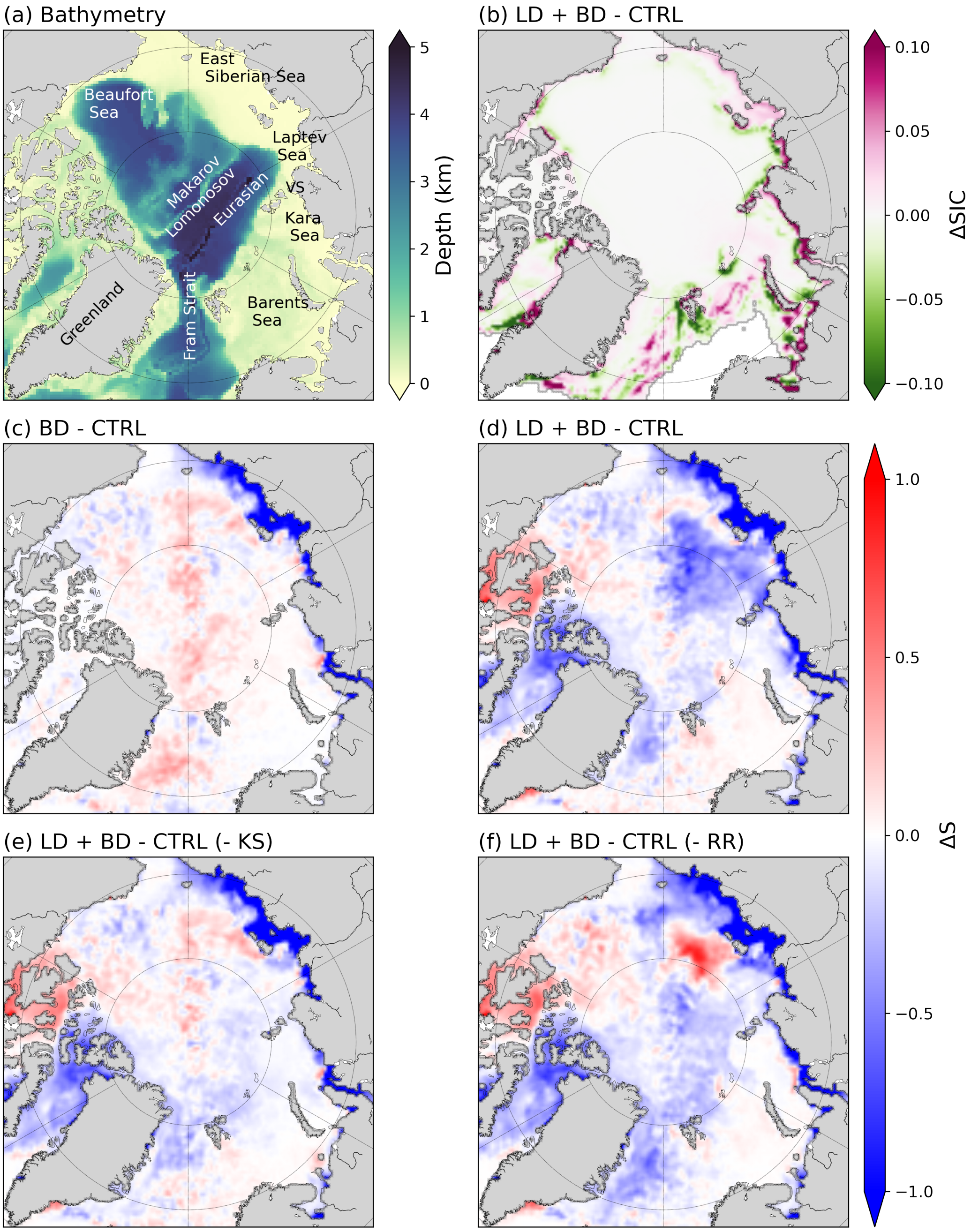

Figure 1. (a) Arctic topography. VS denotes the Vilkitsky Strait. (b) Sea ice concentration difference between LD+BD and CTRL simulations for the mean April of 2006–2015. (c)–(f) Depth averaged (0–40 m) salinity differences for the mean April of 2006–2015 between: (c) the simulation with basal drag parameterization (BD, with landfast ice in the shallow regions) and the CTRL run; (d) the simulation with lateral and basal drag parameterization (LD+BD, with landfast ice in both shallow and deep regions) and the CTRL run; (e) the LD+BD with lateral drag parameterization everywhere except in the Kara Sea and the CTRL run; (f) LD+BD and CTRL simulations as in (d), but without river runoff in the Kara Sea.

ulation (Figure 1c), which is consistent with previous results (Itkin et al., 2015), where the landfast ice parameterization was also depth-dependent and only active in shallow (<30 m) water. During offshore wind events in the East Siberian Sea, new ice formation at the edge of the landfast ice leaves more salt behind and increases the surface ocean salinity in the coastal polynyas. The lateral drag parameterization leads to additional landfast ice in the Kara Sea and around Greenland, where the water is deeper. In contrast to the landfast ice effects in the shallow East Siberian and Laptev Seas, this landfast ice in the deep marginal seas leads to a much fresher upper ocean in the Kara Sea and also Makarov Basin (Figure 1d). We emphasize that the only difference between the BD and LD+BD simulation is the additional landfast ice parameterization in the sea ice component of our model.

Salinity observations in the Arctic are sparse. For example, in the Unified Database for Arctic and Subarctic Hydrography (UDASH, Behrendt et al., 2017; Behrendt et al., 2018), there are only 28 salinity casts in all Aprils of 2006–2015 in the region between the meridians 120°E and 180°E and north of 75°N (approximately the Makarov Basin). Of these 28 casts, only 20 contain data in the upper 40 m. We compare the average over the top 40 m to the corresponding model grid points and find that the root-mean-square difference (RMSD) of salinity between the LD+BD run and the UDASH data (1.06) is smaller than the value between the CTRL run and the UDASH data (1.27). This shows that the extra fast ice in the Kara Sea and the consequential negative salinity anomaly in the Makarov Basin slightly, and maybe fortuitously, reduces a model bias (plots not shown).

In two sensitivity experiments, we turned off the lateral drag parameterization in the LD+BD simulation in the Kara Sea (LD + BD - KS, Figure 1e) and the Greenland Sea and the Canadian Arctic Archipelago separately by setting the coefficient of the lateral drag parameterization to zero in these regions. The fresh upper ocean signal in the Makarov and Eurasian Basins disappears when there is no landfast ice in the Kara Sea

(Figure 1e), whereas the fresh signal in the upper ocean near the Canadian Arctic Archipelago (CAA) and the Greenland Sea disappears when turning off the lateral drag parameterization locally along these coasts (not shown). In a different sensitivity experiment we disabled the river runoff from the Ob and Yenisei Rivers in the Kara Sea aiming to identify the source for the fresher upper ocean signal in the central Arctic (Figure 1f). The amplitude of the negative salinity anomaly in the Kara Sea and the Makarov Basin decreases without river runoff in the Kara Sea and a positive anomaly appears north of the New Siberian Island (Figure 1f). Furthermore, the positive salinity anomaly north of the East Siberian Sea intensifies. We hypothesize that the river runoff contributes to the transport of the low salinity signal in the upper ocean from the Kara Sea to the Makarov Basin (Figure 2).

We trace the river runoff of the Ob and Yenisei Rivers in the Kara Sea with a passive tracer. The passive tracer leaves the Kara Sea through the Vilkitsky Strait (between the Laptev and Kara Seas), then part of the tracer enters the Laptev Sea, and the rest subducts into the Amundsen Basin, passes the Lomonosov Ridge and enters the Makarov Basin. Over the Lomonosov Ridge, Ob/Yenisei water outcrops at the surface and submerges to 50 m in the Makarov Basin (Figure 2). The passive tracer of the Ob and Yenisei water has a similar distribution to the observed Ob/Yenisei water based on chemical tracer-based water mass analyses (Paffrath et al., 2021). The tracer pattern is very similar to the pattern of the low salinity signal in the upper ocean implying a transport path from the Kara Sea to the Makarov Basin.

3.2 Propagation of the low salinity signal

A Hovmöller diagram of the depth-averaged (0–40 m) salinity and salinity difference between different experiments along the transect in Figure 2a illustrates the transport of the low salinity signal from the Kara Sea to the Chuckchi Sea (Figure 3). The positive salinity difference between the BD and CTRL simulations in the Makarov Basin (approximately 1900 km away from the Kara Sea) develops locally very soon after 2001

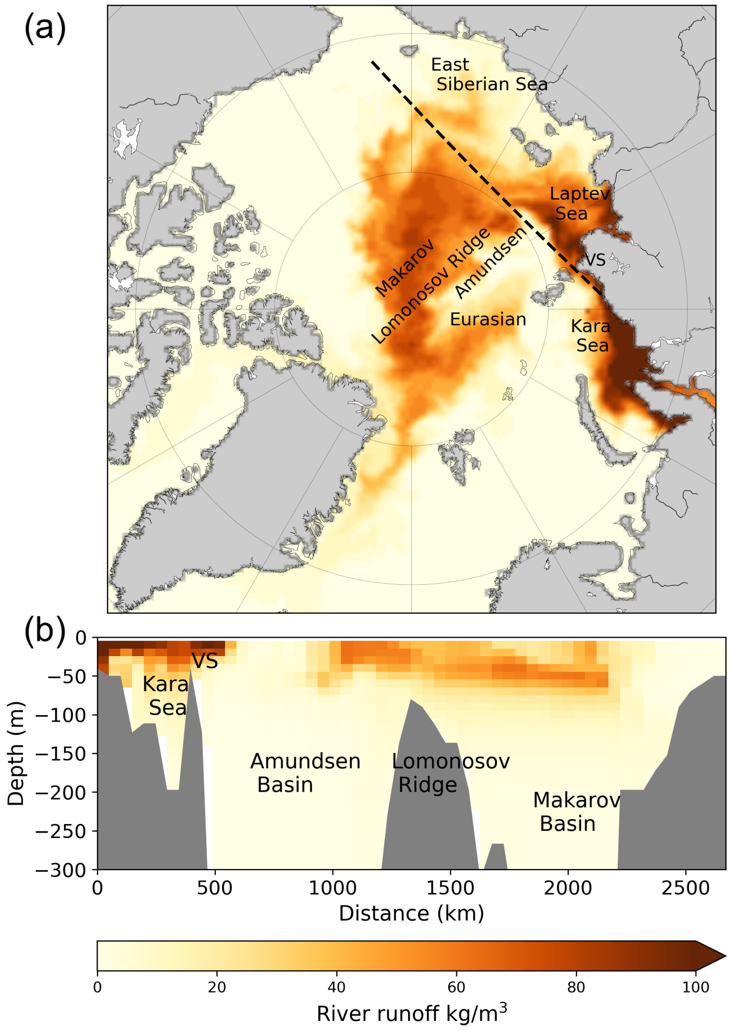

Figure 2. (a) Depth averaged (0–40 m) passive tracer of the river runoff from the Kara Sea in April 2015. (b) Vertical distribution of the passive tracer along the section in panel (a) starting from the Kara Sea to the Chukchi Sea.

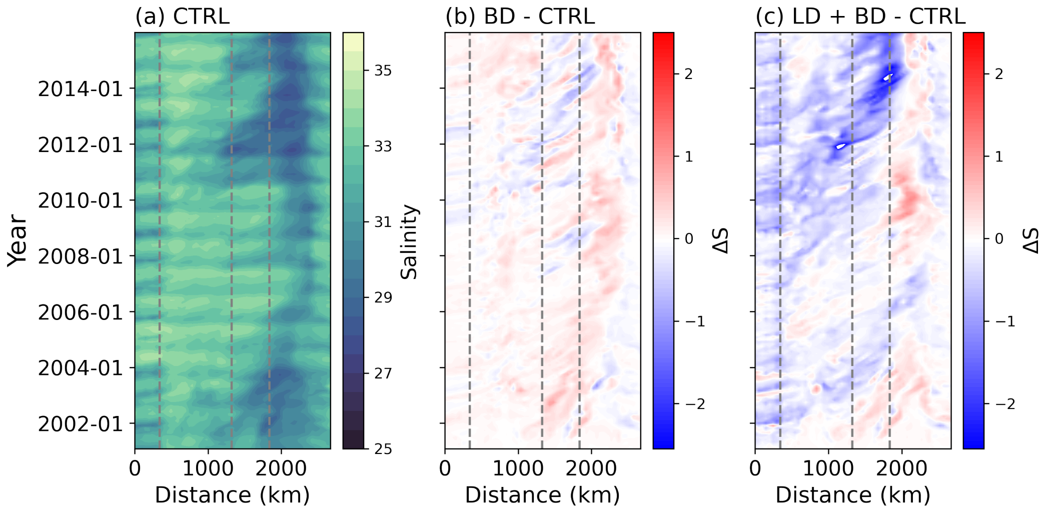

Figure 3. Hovmöller diagram for years 2001 to 2015 of depth-averaged (0–40m) (a) salinity in the CTRL simulation; (b) salinity difference between the BD and CTRL simulations; (c) salinity difference between the LD+BD and CTRL simulations. The abscissa is the distance in km along the transect in Figure 2a. The dashed lines parallel to the ordinate indicate the locations of the Vilkitsky Strait, the Eurasian and the Makarov Basins.

(Figure 3b), when the new ice formation releases salt in the upper ocean in the polynyas north of the East Siberian Sea landfast ice edge. The same positive salinity anomaly also appears in the LD+BD simulation in the Makarov Basin (Figure 3c). In contrast to the locally generated signal, the low salinity signal in the LD+BD simulation in the Makarov and Eurasian Basins is advected from the Kara Sea, apparently starting in 2008, with a negative salinity anomaly peak in 2012. Note the pulses of negative salinity anomaly in the upper ocean moving from the Kara Sea to the Makarov Basin throughout the years 2001-2007. The explanation for the events is elaborated in Section 4.

3.3 Salt budget analysis

Integrating the salt conservation equation leads to a salt budget equation. The change in salt content over time (G^S_{tot}) is equal to the convergence of the advective (G^S_{adv}) and diffusive fluxes (G^S_{diff}), and a forcing term associated with surface salt exchanges (G^S_{forc}):

$$\underbrace{\frac{\partial s}{\partial t}}_{G^S_{\mathrm{tot}}} = \underbrace{-\rho \oint_A uS\,da}_{G^S_{\mathrm{adv}}} + \underbrace{\rho \iiint F_{\mathrm{diff}}\,dx\,dy\,dz}_{G^S_{\mathrm{diff}}} + \underbrace{\rho \iint F_{\mathrm{forc}}\,dx\,dy}_{G^S_{\mathrm{forc}}}, \tag{1}$$

where $\mathbf{u}$ is the ocean velocity normal to the area, S is the salinity, $s = \rho \iiint S\,dx\,dy\,dz$ is the salt content (in grams), da is the area element, A is the surface area of the volume integral. The differences between the simulation with landfast ice and the CTRL run in the advection and salinity tendency in the Arctic Ocean are small for the first five years until the end of 2005 (Figure 4). The trend of the influence of landfast ice in the deep region gradually intensifies after 2006, and the trend stabilizes after the year 2014. The salt content difference in the Arctic Ocean with landfast ice parameterization is determined by surface forcing, advection, and diffusion. The decrease in salt content in the Arctic Ocean in the simulation with fast ice in shallow and deep regions is to 90% caused by changes in advective salt flux through the open boundaries (Figure 4). Furthermore, the remaining 10% of reduced salinity is mainly caused by the surface forcing. The surface forcing flux difference between the LD+BD and CTRL simulation in the Arctic Ocean has a strong seasonal signal governed by the sea ice formation and melt. For perspective, the total salt loss in the Makarov Basin in the upper 40 m is approximately 1.94 Gt per year.

4 Discussion

The presence of landfast ice in sea ice-ocean models changes the position of offshore polynyas and hence the location where sea ice is formed over open water. The modified freshwater flux changes the salinity forcing which in turn leads to changes in the halocline stability in the Arctic (Itkin et al., 2015). This result was obtained with a numerical model that did not have any landfast ice in the Kara Sea. We used a lateral drag parameterization designed to make the Kara Sea landfast ice cover more realistic (Liu et al., 2022) as a switch. When switched on, there is more landfast ice in the Kara Sea, but the landfast ice cover in other fast ice regions does not change very much (Liu et al.,

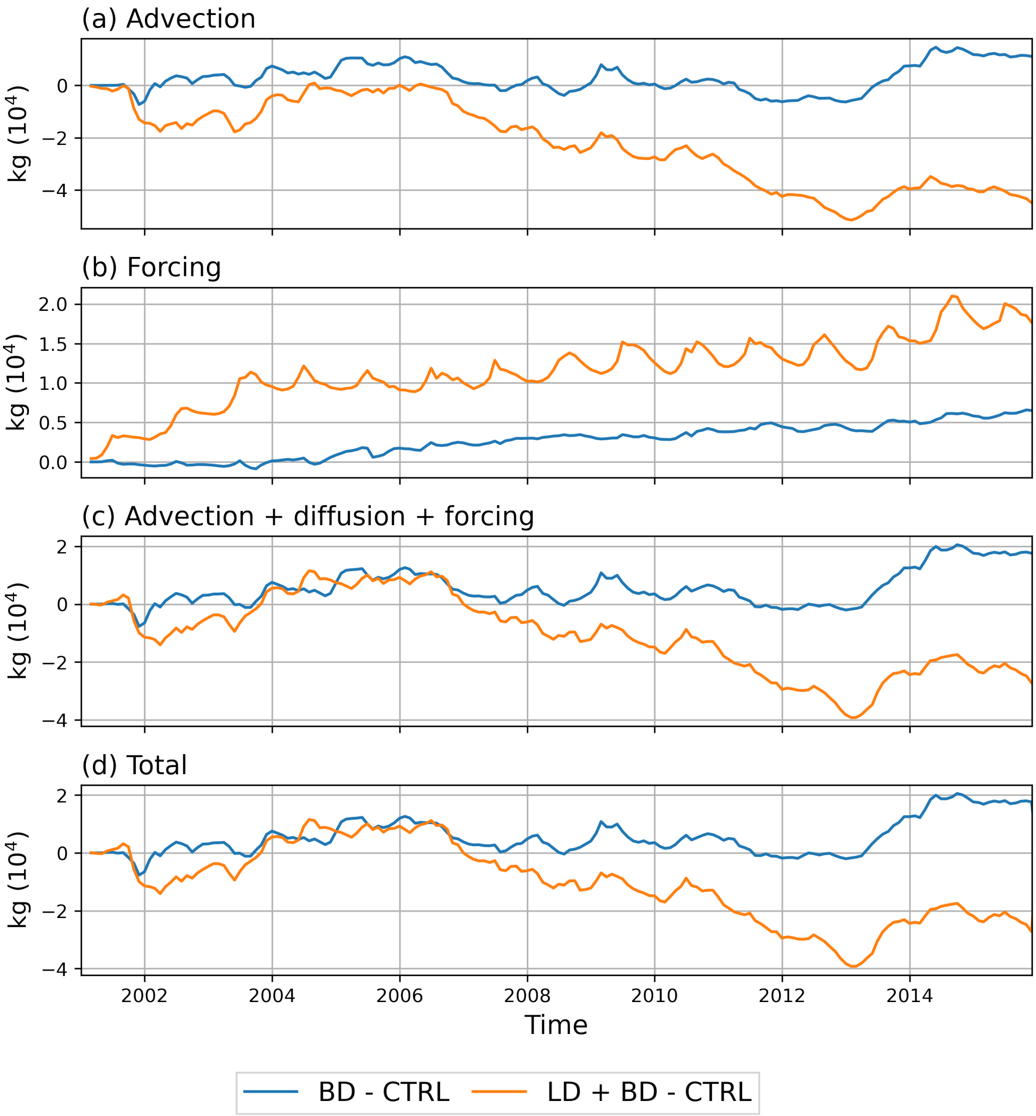

Figure 4. Time series of accumulated salt budget differences ($\int_0^t G(t')\,dt'$, see Eq. 1) in the Arctic Ocean in 2001-2015. The blue line is the difference between BD and CTRL simulation (effects from landfast ice in the shallow region), and the orange line is the difference between LD+BD and CTRL simulation (effects of fast ice in both shallow and deep regions). (a) Advection. (b) Surface forcing (evaporation-precipitation-runoff). (c) The sum of surface forcing, advection and diffusion. (d) Total salt content tendency in the Arctic Ocean. Positive means increasing salinity in the ocean. The (vertical) diffusion term is very small, thus not shown in the plot.

2022). This makes it possible to isolate the effects of the Kara Sea landfast ice. The effect on the near-surface salinity is much larger than including landfast ice in the other marginals seas (Laptev, East Siberian, Beaufort Sea), even though the Kara Sea area is small compared to the other marginal seas. For the halocline, the large decrease of salinity in the top 40 m of the water column means increased stability (and it corrects a saline model bias). Likewise, less landfast ice in the Kara Sea (e.g., in response to climate change), may lead to reduced stability in the central Arctic Ocean and hence an accelerated "Atlantification" as it may become easier for warm Atlantic water to reach the surface (Asbjørnsen et al., 2020; Ingvaldsen et al., 2021), with significant consequences for the sea ice cover extent and seasonality.

Although the negative salinity anomaly in the upper ocean in the simulation with fast ice in the Kara Sea travels from the Kara Sea to the Makarov Basin soon after the start of the model run, there are two main transport episodes (2002–2006 and 2008–2015). These may be driven by the wind forcing in the Arctic (Duan et al., 2019; Zatsepin et al., 2017). The negative salinity difference in the upper ocean is largest after the end of summer in 2012 (Figure 3c), presumably because of the large sea ice retreat in 2012. In August 2012, an intense storm increased mixing in the ocean boundary layer, increased upward ocean heat transport, causing bottom melt, and reduced the sea ice volume about twice as fast as in other years (Zhang et al., 2013). Eventually, the sea ice extent at the end of the summer in 2012 was smaller than it had been in the previous 33 years (Parkinson & Comiso, 2013). The processes are also at play in our simulation and the mean simulated sea ice extent reaches its lowest value of the simulation in 2012 (not shown). More landfast ice melting in the LD+BD simulation reduces the salinity in the upper ocean compared to the CTRL simulation. The increased mixing and melting increase the negative salinity difference. The particularly fresh upper ocean in 2012 may also be related to position of the Beaufort Gyre. As a major freshwater reservoir for the Arctic Ocean, the gyre extended northward after 2012, thus increasing the freshwater content in the Makarov Basin, and making the central Arctic Ocean fresher (Bertosio et al., 2022).

The Kara Sea receives freshwater discharge from the Ob and Yenisei Rivers, which carry over one-third of the total freshwater discharge in the Arctic (Janout et al., 2015). The geostrophic surface currents determine the circulation pathways of river runoff, and of surface water originally from the Pacific and the Atlantic Oceans (Wang et al., 2021). The simulated passive tracer for Ob/Yenisei water agrees with the observed Ob/Yenisei water distribution (Laukert et al., 2017; Paffrath et al., 2021). The tracer experiment demonstrates that the river runoff and the negative salinity anomaly in the upper ocean induced by the fast ice in the Kara Sea travel from the Kara Sea to the Makarov Basin via the Vilkitsky Strait. The exact mechanism by which the river runoff in the Kara Sea modifies the influence the landfast ice has on the hydrography cannot be extracted from the numerical model because the Ob/Yenisei water is stored in landfast ice during sea ice formation and the riverine heat, which is not taken into account in our model, is assumed to be important to explain the phenomena (Janout et al., 2020).

The Arctic mixed layer is important to physical, chemical, and biological processes. Mixed layer properties also influence ocean stratification, sea ice distribution, and heat transfer between ocean, sea ice, and atmosphere. Peralta-Ferriz and Woodgate (2015) suggested two drivers for seasonal mixed layer depth change: sea ice thermodynamics (i.e., salt rejection during ice formation, freshwater input during the ice melt) and wind-driven mixing. During ice-free phases, wind-driven mixing deepens the mixed layer, while thermodynamic processes dominate the stratification and control mixed layer depth variability in winter. With more fast ice less salt is released into the ocean which may modify the mixed layer depth. Our model configuration has 50 vertical layers with a minimum thickness of 10 m in the upper ocean, which is insufficient to explore the details of the influence of landfast ice parameterization on the mixed layer depth. Vertical grid refinement in the upper ocean would allow studying the mixed layer variability difference with and without the landfast ice parameterization.

A proper representation of the landfast ice distribution, as suggested here, may be even more important in the Southern Ocean than in the Arctic Ocean. Along the deep Southern Ocean shelf around Antarctica, landfast ice is mainly attached to grounded icebergs or other coastal features (e.g. the shoreline, glacier tongues, and ice shelves, Fraser et al., 2012, 2020). Salt rejection during continuous sea-ice formation (in polynyas) on the shelves produces the densest waters observed in the world ocean, which eventually are a source of Antarctic Bottom water (Williams et al., 2010; Ohshima et al., 2013, 2016). The dense bottom water is an important part of the global circulation (Killworth, 1983; Nihashi & Ohshima, 2015; Ohshima et al., 2016). In this sense, the impact of realistically simulated landfast ice around Antarctica may even be larger than in the Arctic Ocean where the hydrographic processes appear to be restricted mainly to surface waters.

5 Conclusion

More landfast ice in the Arctic Ocean decreases the upper ocean salinity locally on the shelves in the Kara, Laptev and East Siberian Seas. The largest effect, however, is found for the Kara Sea, where the large fresh upper ocean signal induced by the landfast ice is transported to the central Arctic Ocean and leads to surprisingly large salinity anomaly which increases the halocline stability. River runoff in the Kara Sea contributes to transporting the signal from the Kara Sea to the Makarov Basin. The negative salinity tendency with the landfast ice in both shallow and deep shelves can be attributed mainly (90%) to advective fluxes out of the Arctic Ocean and to surface forcing (10%).

A sea ice model with a proper representation of landfast ice will improve our understanding of its influence on the hydrography in the Arctic. The landfast ice occurrence modifies sea ice thermodynamics and thus may reshape the mixed layer depth. A finner vertical resolution model is suggested to investigate further the impact of landfast ice presentation on the mixed layer depth. Implementing landfast ice parameterizations in sea ice model of the Antarctic will allow to explore the effects of landfast ice on the Antarctic Bottom Water formation.

Open Research

The model data in this manuscript is based on the Massachusetts Institute of Technology general circulation model (MITgcm, MITgcm Group, 2022), the version with lateral drag parameterization is available at `https://doi.org/10.5281/zenodo.7954400` and the model configurations at `https://doi.org/10.5281/zenodo.7919422`. The salinity in the Unified Database for Arctic and Subarctic Hydrography (UDASH) is available from the PANGAEA data archive (Behrendt et al., 2017). Figures are made with Matplotlib version 3.1.3 (Hunter, 2007), available under the Matplotlib license at `https://matplotlib.org/`.

Acknowledgments

The authors thank Markus Janout, Thomas Jung, and Lars Kaleschke for constructive discussions. This work is supported by the DFG-funded International Research Training Group ArcTrain (IRTG 1904 ArcTrain).

References

Asbjørnsen, H., Årthun, M., Skagseth, Ø., & Eldevik, T. (2020). Mechanisms underlying recent Arctic Atlantification. *Geophysical research letters*, *47*(15), e2020GL088036. doi: 10.1029/2020GL088036

Behrendt, A., Sumata, H., Rabe, B., & Schauer, U. (2017). *A comprehensive, quality-controlled and up-to-date data set of temperature and salinity data for the Arctic Mediterranean Sea (Version 1.0)* [data set]. PANGAEA. doi: 10.1594/PANGAEA.872931

Behrendt, A., Sumata, H., Rabe, B., & Schauer, U. (2018). UDASH–Unified Database for Arctic and Subarctic Hydrography. *Earth System Science Data*, *10*(2), 1119–1138. doi: 10.5194/essd-10-1119-2018

Bertosio, C., Provost, C., Athanase, M., Sennéchael, N., Garric, G., Lellouche, J.-m., … Park, T. (2022). Changes in freshwater distribution and pathways in the Arctic Ocean since 2007 in the Mercator Ocean global operational system. *Journal of Geophysical Research: Oceans*, *127*(6), e2021JC017701. doi: 10.1029/2021JC017701

Dee, D. P., Uppala, S. M., Simmons, A. J., Berrisford, P., Poli, P., Kobayashi, S., … Vitart, F. (2011). The ERA-Interim reanalysis: Configuration and performance of the data assimilation system. *Quarterly Journal of the Royal Meteorological Society*, *137*(656), 553–597. doi: 10.1002/qj.828

Divine, D. V., Korsnes, R., Makshtas, A. P., Godtliebsen, F., & Svendsen, H. (2005). Atmospheric-driven state transfer of shore-fast ice in the northeastern Kara Sea. *Journal of Geophysical Research C: Oceans*, *110*(9), 1–13. doi: 10.1029/2004JC002706

Duan, C., Dong, S., Xie, Z., & Wang, Z. (2019). Temporal variability and trends of sea ice in the Kara Sea and their relationship with atmospheric factors. *Polar Science*, *20*, 136–147. doi: 10.1016/j.polar.2019.03.002

Fraser, A. D., Massom, R. A., Michael, K. J., Galton-Fenzi, B. K., & Lieser, J. L. (2012). East Antarctic landfast sea ice distribution and variability, 2000–08. *Journal of Climate*, *25*(4), 1137–1156. doi: 10.1175/JCLI-D-10-05032.1

Fraser, A. D., Massom, R. A., Ohshima, K. I., Willmes, S., Kappes, P. J., Cartwright, J., & Porter-Smith, R. (2020). High-resolution mapping of circum-Antarctic landfast sea ice distribution, 2000-2018. *Earth System Science Data*, *12*(4), 2987–2999. doi: 10.5194/essd-12-2987-2020

Haine, T. W., Curry, B., Gerdes, R., Hansen, E., Karcher, M., Lee, C., … Woodgate, R. (2015). Arctic freshwater export: Status, mechanisms, and prospects. *Global and Planetary Change*, *125*, 13–35. doi: 10.1016/j.gloplacha.2014.11.013

Hibler, W. D. (1979). A dynamic thermodynamic sea ice model. *Journal of Physical Oceanography*, *9*(4), 815–846. doi: 10.1175/1520-0485(1979)009⟨0815:ADTSIM⟩2.0.CO;2

Hunter, J. D. (2007). Matplotlib: A 2d graphics environment. *Computing in Science & Engineering*, *9*(3), 90–95. doi: 10.5281/zenodo.3633844

Ingvaldsen, R. B., Assmann, K. M., Primicerio, R., Fossheim, M., Polyakov, I. V., & Dolgov, A. V. (2021). Physical manifestations and ecological implications of Arctic Atlantification. *Nature Reviews Earth & Environment*, *2*(12), 874–889. doi: 10.1038/s43017-021-00228-x

Itkin, P., Losch, M., & Gerdes, R. (2015). Landfast ice affects the stability of the Arctic halocline: Evidence from a numerical model. *Journal of Geophysical Research: Oceans*, *120*(4), 2622–2635. doi: 10.1002/2014JC010353

Janout, M. A., Aksenov, Y., Hölemann, J. A., Rabe, B., Schauer, U., Polyakov, I. V., … Timokhov, L. (2015). Kara Sea freshwater transport through Vilkitsky Strait: Variability, forcing, and further pathways toward the western Arctic Ocean from a model and observations. *Journal of Geophysical Research: Oceans*, *120*(7), 4925–4944. doi: 10.1002/2014JC010635

Janout, M. A., Hölemann, J., Laukert, G., Smirnov, A., Krumpen, T., Bauch, D., & Timokhov, L. (2020). On the variability of stratification in the freshwater-influenced Laptev Sea region. *Frontiers in Marine Science*, *7*, 543489. doi: 10.3389/fmars.2020.543489

Johnson, M., Proshutinsky, A., Aksenov, Y., Nguyen, A. T., Lindsay, R., Haas, C., … De Cuevas, B. (2012). Evaluation of Arctic sea ice thickness simulated by Arctic Ocean model intercomparison project models. *Journal of Geophysical Research: Oceans*, *117*(3). doi: 10.1029/2011JC007257

Killworth, P. D. (1983). Deep convection in the World Ocean. *Reviews of Geophysics*, *21*(1), 1–26. doi: 10.1029/RG021i001p00001

Laukert, G., Frank, M., Bauch, D., Hathorne, E. C., Rabe, B., von Appen, W.-J., …

Kassens, H. (2017). Ocean circulation and freshwater pathways in the Arctic Mediterranean based on a combined Nd isotope, REE and oxygen isotope section across Fram Strait. *Geochimica et Cosmochimica Acta*, *202*, 285–309. doi: 10.1016/j.gca.2016.12.028

Lemieux, J. F., Dupont, F., Blain, P., Roy, F., Smith, G. C., & Flato, G. M. (2016). Improving the simulation of landfast ice by combining tensile strength and a parameterization for grounded ridges. *Journal of Geophysical Research: Oceans*, *121*(10), 7354–7368. doi: 10.1002/2016JC012006

Lemieux, J. F., Tremblay, L. B., Dupont, F., Plante, M., Smith, G. C., & Dumont, D. (2015). A basal stress parameterization for modeling landfast ice. *Journal of Geophysical Research: Oceans*, *120*(4), 3157–3173. doi: 10.1002/2014JC010678

Liu, Y., Losch, M., Hutter, N., & Mu, L. (2022). A new parameterization of coastal drag to simulate landfast ice in deep marginal seas in the Arctic. *Journal of Geophysical Research: Oceans*, *127*(6), e2022JC018413. doi: 10.1029/2022JC018413

Losch, M., Menemenlis, D., Campin, J. M., Heimbach, P., & Hill, C. (2010). On the formulation of sea-ice models. Part 1: Effects of different solver implementations and parameterizations. *Ocean Modelling*, *33*(1-2), 129–144. doi: 10.1016/j.ocemod.2009.12.008

Mahoney, A. R., Eicken, H., Gaylord, A. G., & Gens, R. (2014). Landfast sea ice extent in the Chukchi and Beaufort Seas: The annual cycle and decadal variability. *Cold Regions Science and Technology*, *103*, 41–56. doi: 10.1016/j.coldregions.2014.03.003

Marshall, J., Adcroft, A., Hill, C., Perelman, L., & Heisey, C. (1997). A finite-volume, incompressible navier stokes model for, studies of the ocean on parallel computers. *Journal of Geophysical Research C: Oceans*, *102*(C3), 5753–5766. doi: 10.1029/96JC02775

MITgcm Group. (2022). *MITgcm User Manual.* `https://mitgcm.readthedocs.io/`. Cambridge, MA 02139, USA.

Morison, J., Kwok, R., Peralta-Ferriz, C., Alkire, M., Rigor, I., Andersen, R., & Steele, M. (2012). Changing Arctic Ocean freshwater pathways. *Nature*, *481*(7379), 66–70. doi: 10.1038/NATURE10705

Nihashi, S., & Ohshima, K. I. (2015). Circumpolar mapping of Antarctic coastal polynyas and landfast sea ice: Relationship and variability. *Journal of Climate*, *28*(9), 3650–3670. doi: 10.1175/JCLI-D-14-00369.1

Ohshima, K. I., Fukamachi, Y., Williams, G. D., Nihashi, S., Roquet, F., Kitade, Y., . . . Wakatsuchi, M. (2013). Antarctic Bottom Water production by intense sea-ice formation in the Cape Darnley polynya. *Nature Geoscience*, *6*(3), 235–240. doi: 10.1038/ngeo1738

Ohshima, K. I., Nihashi, S., & Iwamoto, K. (2016). Global view of sea-ice production in polynyas and its linkage to dense/bottom water formation. *Geoscience Letters*, *3*(1). doi: 10.1186/s40562-016-0045-4

Paffrath, R., Laukert, G., Bauch, D., Rutgers van der Loeff, M., & Pahnke, K. (2021). Separating individual contributions of major Siberian rivers in the Transpolar Drift of the Arctic Ocean. *Scientific Reports*, *11*(1), 1–11. doi: 10.1038/s41598-021-86948-y

Parkinson, C. L., & Comiso, J. C. (2013). On the 2012 record low Arctic sea ice cover: Combined impact of preconditioning and an August storm. *Geophysical Research Letters*, *40*(7), 1356–1361. doi: 10.1002/grl.50349

Peralta-Ferriz, C., & Woodgate, R. A. (2015). Seasonal and interannual variability of pan-Arctic surface mixed layer properties from 1979 to 2012 from hydrographic data, and the dominance of stratification for multiyear mixed layer depth shoaling. *Progress in Oceanography*, *134*, 19–53. doi: 10.1016/j.pocean.2014.12.005

Proshutinsky, A., Dukhovskoy, D., Timmermans, M.-L., Krishfield, R., & Bamber,

J. L. (2015). Arctic circulation regimes. *Philosophical Transactions of the Royal Society A: Mathematical, Physical and Engineering Sciences*, *373*(2052), 20140160. doi: 10.1098/rsta.2014.0160

Rudels, B., Jones, E., Anderson, L., & Kattner, G. (1994). On the intermediate depth waters of the Arctic Ocean. *Washington DC American Geophysical Union Geophysical Monograph Series*, *85*, 33–46.

Semtner, A. J. (1976). A model for the thermodynamic growth of sea ice in numerical investigations of climate. *Journal of Physical Oceanography*, *6*(3), 379–389. doi: 10.1175/1520-0485(1976)006⟨0379:amfttg⟩2.0.co;2

Serreze, M. C., Barrett, A. P., Slater, A. G., Woodgate, R. A., Aagaard, K., Lammers, R. B., … Lee, C. M. (2006). The large-scale freshwater cycle of the Arctic. *Journal of Geophysical Research: Oceans*, *111*(11). doi: 10.1029/2005JC003424

Steele, M., Ermold, W., & Zhang, J. (2011). Modeling the formation and fate of the near-surface temperature maximum in the Canadian Basin of the Arctic Ocean. *Journal of Geophysical Research: Oceans*, *116*(11), 1–13. doi: 10.1029/2010JC006803

Timmermans, M. L., & Marshall, J. (2020). Understanding Arctic Ocean circulation: A review of ocean dynamics in a changing climate. *Journal of Geophysical Research: Oceans*, *125*(4). doi: 10.1029/2018JC014378

Ungermann, M., & Losch, M. (2018). An observationally based evaluation of subgrid scale ice thickness distributions simulated in a large-scale sea ice-ocean model of the Arctic Ocean. *Journal of Geophysical Research: Oceans*, *123*(11), 8052–8067. doi: 10.1029/2018JC014022

Wang, Q., Danilov, S., Sidorenko, D., & Wang, X. (2021). Circulation pathways and exports of Arctic river runoff influenced by atmospheric circulation regimes. *Frontiers in Marine Science*, *8*, 707593. doi: 10.3389/fmars.2021.707593

Williams, G. D., Aoki, S., Jacobs, S. S., Rintoul, S. R., Tamura, T., & Bindoff,

N. L. (2010). Antarctic bottom water from the Adélie and George V Land coast, East Antarctica (140-149°E). *Journal of Geophysical Research: Oceans*, *115*(4), 1–29. doi: 10.1029/2009JC005812

World Meteorological Organization. (1970). *WMO sea-ice nomenclature. Terminology, codes and illustrated glossary* (Tech. Rep.). Geneva: Secretariat of the World Meteorological Organization.

Zatsepin, A., Zavialov, P., Baranov, V., Kremenetskiy, V., Nedospasov, A., Poyarkov, S., & Ocherednik, V. (2017). On the mechanism of wind-induced transformation of a river runoff water lens in the Kara Sea. *Oceanology*, *57*(1), 1–7. doi: 10.1134/S0001437017010222

Zhang, J., & Hibler, W. D. (1997). On an efficient numerical method for modeling sea ice dynamics. *Journal of Geophysical Research: Oceans*, *102*(C4), 8691–8702. doi: 10.1029/96JC03744

Zhang, J., Lindsay, R., Schweiger, A., & Steele, M. (2013). The impact of an intense summer cyclone on 2012 Arctic sea ice retreat. *Geophysical Research Letters*, *40*(4), 720–726. doi: 10.1002/grl.50190